Morphological and functional analyses of skeletal muscles
from an immunodeficient animal model of limb girdle muscular dystrophy type 2E

Gaia Giovannelli[1], PhD; Giorgia Giacomazzi[2], MSc; Hanne Grosemans[2], B.S and Maurilio Sampaolesi, PhD[2,3] (iD)

[1]*Department of Neurosciences and Imaging, "G. d'Annunzio" University, Chieti, Italy;*
[2]*Translational Cardiomyology, Stem Cell Research Institute, Catholic University of Leuven, Herestraat 49 B-3000 Leuven, Belgium;*
[3]*Division of Human Anatomy, Dept. of Public Health, Experimental and Forensic Medicine, University of Pavia, 27100 Pavia, Italy.*

Correspondence to:
Prof. Dr. Maurilio Sampaolesi
Translational Cardiomyology Lab
KU Leuven, Herestraat 49 – O&N4 – bus 814
3000 Leuven, Belgium
maurilio.sampaolesi@kuleuven.be

- Running title: Sgcb/Rag2/γc-null muscle analysis

- Number of words in abstract: 141
- Number of words in manuscript: **3838**

- None of the authors has any conflict of interest to disclose.
- We confirm that we have read the Journal's position on issues involved in ethical publication and affirm that this report is consistent with those guidelines

Acknowledgement

Abstract

Introduction - Limb-girdle muscular dystrophy type 2E (LGMD 2E) is caused by mutations in the β-sarcoglycan gene, which is expressed in skeletal, cardiac and smooth muscle. β-sarcoglycan deficient (Sgcb-null) mice develop severe muscular dystrophy and cardiomyopathy with focal areas of necrosis.

Methods - We performed morphological (histological and cellular characterization) and functional (isometric tetanic force and fatigue) analyses in dystrophic mice. Comparisons studies were carried out in 1-month-old (clinical onset of the disease) and 7-month-old mice among controls (C57/BL6, Rag2/γc-null), immunocompetent and immunodeficient dystrophic mice (Sgcb-null, Sgcb/Rag2/γc-null mice respectively).

Results – We provide evidence that the lack of an immunological system results in an increase in the calcification area in striated muscle without impairing extensor digitorum longus muscle performances. Sgcb/Rag2/γc-null muscles showed a significant reduction of AP+ mesoangioblasts.

Discussion – The immunological system counteracts skeletal muscle degeneration in a murine model of LGMD 2E.

Key words: β-sarcoglycan; immunodeficient dystrophic mice; EDL; mesoangioblasts; smooth muscle.

Introduction

In skeletal and cardiac muscle, dystrophin is associated with sarcolemmal and cytoskeletal proteins [1] forming the dystrophin–glycoprotein complex (DGC), which provides a structural link between laminin 2 in the extracellular matrix and the actin-based intracellular cytoskeleton [2]. Thus, dystrophin is a linkage between the outside and the inside of muscle cells, protecting them from contraction-induced damage [3-5].

Mutations in genes encoding several components of the DGC have been associated with muscular dystrophies [1] which are a heterogeneous group of disorders characterized by progressive skeletal muscle wasting and weakness. Cardiac involvement is common in muscular dystrophies, but is not necessarily related to the degree of skeletal myopathy [6]. Several proteins contribute to the stability of the DGC complex, and among those, sarcoglycans constitute important elements. Sarcoglycans ($\alpha,\beta,\delta,\varepsilon,\gamma,\zeta$) are transmembrane proteins that form a heteromeric complex [3], which is part of the DGC [5]. Mutations in sarcoglycan genes cause autosomal recessive limb-girdle muscular dystrophies (LGMD2) (types C-F) [3,7,8]. In particular, LGMD type 2E is caused by mutations in the β-sarcoglycan gene [5] and is characterized by pelvic muscle weakness, early scapular winging, severe dilated cardiomyopathy and lethal ventricular arrhythmias [9]. Mouse models of all sarcoglycanopathies have been developed, including Sgcb-null mice that demonstrate the disruption of the sarcoglycan and dystroglycan complexes in skeletal, cardiac, and smooth muscles, resulting in severe muscular dystrophy, cardiomyopathy, and vascular abnormalities. Pathological features of Sgcb-null skeletal muscles are fibre necrosis, calcification, fibrosis and fatty infiltration [3,9].

Loss of cells and injury in skeletal and cardiac muscles are associated with a regenerative process driven by the final interaction among resident stem cells and differentiated cells. Satellite cells are skeletal muscle quiescent progenitors, activated during physiological muscle growth or after an injury [10]. Despite their high myogenic capacities, there are limitations in the use of satellite cells for muscle regeneration, such as difficulty of cell migration from the sites of injection and the loss of regenerative efficiency following in vitro expansion [11]. Alongside satellite cells, other cell types have been described for muscle regeneration. Mesoangioblasts (MABs) are vessel associated cells capable of differentiating into several mesodermal lineages, including skeletal muscle and smooth muscle cells [12-15]. Moreover, MABs constitute an interesting source for stem cell therapies given their renewal abilities and migration properties, and they were characterized also from cardiac tissues [13,15,16]. Fibro adipogenic progenitors (FAPs) have been found to modulate myogenesis and eventually adipogenesis [17]. Alongside the variety of stem cells that can potentially contribute to the regeneration process, infiltrating inflammatory and immune cells (neutrophils, macrophages,

lymphocytes) hold a crucial role in the regeneration process. Acute skeletal muscle injury causes an immediate transient wave of neutrophils followed by a more persistent infiltration of M1 (pro-inflammatory) and M2 (anti-inflammatory/pro-regenerative) macrophages. Injured skeletal muscles are also colonized by different population of T cells including helper T lymphocytes (ThL), which have both anti- and pro-fibrotic role [18]; cytotoxic T lymphocytes (TcL), responsible for inflammatory response (promoted eosinophilia [19] and fibrosis [20,21]; regulatory T lymphocytes (Treg L), which in turn control the inflammatory response, by promoting the M1/M2 switch, and the activation of satellite cells [22].

Previous investigations on animal models of Duchene muscular dystrophy (DMD) have shown that cellular immune responses by TcL and ThL contribute to muscle pathology, and that removal of specific lymphoid cell populations can reduce muscle pathology. In addition, innate immune responses may also promote muscular dystrophy by the infiltration of myeloid cell populations into the dystrophic muscle. Collectively, the previous observations suggest that the contribution of the immune system to muscular dystrophy may be significant, and that therapeutic approaches based upon immune interventions may ameliorate the pathological progression of dystrophin and sarcoglycan deficiencies [20,21].

In Sgcb-null mice death occurs by heart failure at the age of 16-18 months [3]. Healing of the infarcted heart is associated with intense angiogenesis. The rapid induction of angiogenic growth factors results in formation of a network of hyperpermeable neovessels that may lack a pericyte coat [23]. As the infarct vasculature matures, some neovessels are coated with pericytes, whereas uncoated vessels regress [24]. Mature coated vessels protected from regression exhibit decreased inflammatory activity and contribute to the scar stabilization [25]. No immunodeficient animal models for LGMD2E are available to evaluate the consequences of immune system deficiency in dystrophic condition. Thus, we have generated the new animal model Sgcb/Rag2/γc-null mouse, which lacks functional T, B and NK cells and is affected by LGMD2E.

The aim of this work was to characterize this new animal model and evaluate if immunodeficiency as described above affected the dystrophic phenotype.

Methods

Animal handling

All protocols were conducted in according to the guidelines of the Animal Welfare Committee of KU Leuven Belgian/European legislation and the Ethical Approval of KU Leuven (P095/2012). The *Sgcb/Rag2/γc*-null mice were generated in our laboratory. C57Bl/6J and *Rag2/γc*-null mice are used as control. Four 1-month old and four 7-month old mice were used per strain.

Histologic analyses

Cardiac and skeletal muscles (gastrocnemius and diaphragm) were collected from 1- and 7-month old C57/BL6, *Rag2/γc*-null, *Sgcb*-null and *Sgcb/Rag2/_c*-null mice. Tissues were fixed in 4% paraformaldehyde and embedded in paraffin or cryoconserved in optimum cutting temperature (OCT) compound (Sakura Tissue-Tek, US) following the manufacturer's instructions. The H&E and Masson trichrome (Sigma-Aldrich, US) staining were performed on 5-μm-thick paraffin-slices and the NADH- transferase staining was performed on 7-μm-thick cryosection as previously reported [26].

Cell isolation.

Cell populations were isolated from hindlimb muscle, including tibialis anterior, gastrocnemius, extensor digitorum longus (EDL) and soleus, and heart biopsies of 1 and 7 month C57/BL6, Rag2/γc-null, Sgcb-null and Sgcb/Rag2/γc-null mice. Biopsies were taken and small pieces (approximately $2 \times 2 \times 2$ mm) were cultured on collagen-coated dishes. When spreading cells appeared from fragments, they were carefully removed and cells were detached with TriplE (Gibco, US). The large part of mixed cell populations obtained from 1- and 7-month old animals was processed by FACS-analysis for sorting AP+ fractions and a small part was plated onto collagen-coated Petri dishes and incubate (at 37°C in a 5% CO2, 5% O2 humidified incubator) for further characterizations. Alkaline phosphatase was used as specific markers to sort pure MABs population as previously described [27]. MABs as AP-positive cell fraction were cultured and expanded on collagen-coated plastic in DMEM-20 culture medium (DMEM high glucose, 20% of fetal calf serum [FCS], 1% penicillin/streptomycin solution [100units], 2 mM glutamine, 1 mM sodium pyruvate, 1x nonessential amino acid solution, 0.5% β–mercaptoethanol). When cells reached 80–85% confluence they were split in a 1:4 ratio. The mixed cell populations were characterized by the AP enzymatic staining by BCT/NBT reagent (Sigma-Aldrich; US). Because we failed to obtain a consistent number of viable cells after cell sorting, mixed cell populations from 7-month old animals were directly plated and expanded for further characterizations.

Differentiation Assays

The smooth muscle differentiation was induced in a mix population and in MABs (AP+ cells) by transforming growth factor β (TGFβ- treatment (DMEM high glucose, 2% of heat-inactivated horse serum [HS], 1% penicillin/streptomycin solution, 2 mM glutamine, 1 mM sodium pyruvate, and 10ng/ml TGFβ, (Peprotech, US). On day 0, $5x10^3$ cells per cm^2, were plated in collagen-coated Petri dishes and incubated at 37°C with DMEM-20 medium. After 24 h cells were washed with PBS, cultured in the smooth muscle differentiation medium, and incubated for 7 days. At the end of differentiation, cultures were fixed with 4% paraformaldehyde (PFA, Sigma Aldrich, US) in PBS.

Immunofluorescence Staining

Immunofluorescence staining was performed following the commonly used steps of Triton-based (Sigma-Aldrich, US) permeabilization and background blocking with donkey serum (Sigma-Aldrich, US). Cells or 7-μm-thick cryosections were incubated overnight with primary antibodies (reported hereafter) at 4°C, and after washing 1 hr of incubation with 1:500 AlexaFluor-conjugated donkey secondary antibodies (Thermo Fisher, US) was performed. Nuclei were counterstained with Hoechst.

Primary antibodies and relative dilutions were: alpha-Smooth Muscle Actin (α-SMA) Cy3™ antibody, Mouse monoclonal (1:200, Sigma-Aldrich, US); calponin, Rabbit monoclonal antibody (1:200, Abcam, UK); F4/80 (a general macrophage marker) (1:200, Abcam, UK); CD206 (mannose receptor) (1:100, Abcam, UK); alkaline phosphatase AP (1:500, R&D system, US); BA-D5 (Myosin heavy chain 1) (Developmental studies hybridoma bank, US); SC-71 (Myosin heavy chain 2A) (Developmental studies hybridoma bank, US). Pictures were acquired with an Eclipse Ti microscope (Nikon) and the morphological analysis was performed with ImageJ software (NIH, USA)

Muscle function by an intact muscle test system

The EDL was immediately excised from each mouse and maintained in a storage solution (Krebs-Ringer bicarbonate buffer ($MgCl_2$, KCl, NaCl, Na_2HPO_4, NaH_2PO_4, D-glucose and $NaHCO_3$) to which was added potassium phosphate (1.2 mM), magnesium sulfate (0.57 mM), calcium chloride (2.00 mM), and HEPES (10.0 mM) and gassed with a mixture of 95% O_2 and 5% CO_2 at room temperature (pH: 7.3 ± 0.3; Osmolarity: $267 \pm 5\%$ mOsm/L) [28,29]. The test was performed in a temperature controlled (30 °C) chamber containing the buffer solution and continuously gassed with a mixture of 95% O_2 and 5% CO_2 [30]. Muscles were mounted vertically in the chamber linked one end to a fixed clamp while the other end to the lever-arm of muscle strength measuring Instruments 300B actuator/transducer system (Aurora Scientific, Canada), using a nylon thread. The compliance of the Nylon thread and the muscle were respectively equal to 0.187 ± 0.004 μm/mN and to 2.000 ± 0.082 μm/mN.

Switching between isometric and isotonic measurements without removing the specimen from the bath was made possible by controlling the force and the position mode of the lever-arm.

Two platinum electrodes located about 2 mm from each side of the isolated muscle allowed electrical stimulation with 200 mA controlled current pulses (pulse voltage of around 10 V). For each experiment, the initial muscle length was adjusted to the length (L_0), which produced the

highest twitch force. The muscle cross-sectional area (CSA) was determined by dividing the muscle mass (m) with the product of the optimal fibre length (L_f) and the density of mammalian skeletal muscle (1.06 mg/mm^3). The L_f was determined by multiplying that value of L_0 for the fibre length to the muscle length ratio (0.44 for the EDL) indicated in the literature [28,31] .

$$L_f(mm) = L_0(mm) \_0.44$$

$$CSA(mm^2) = \frac{m(mg)}{Lf(mm)\_1.06(mg/mm^3)}$$

The protocol allowed measurement of isometric and isotonic parameters, inducing the maximum force and the fatigue sequence.

The muscle was initially stimulated with a 0.5 ms single pulse to measure the isometric twitch force and contraction time. A second pulse was applied to check the consistency of the values obtained and to balance muscle equilibration before applying tetanic stimulation.

The muscle was then subjected to a first train (0.6 s at 120 Hz) to induce unfused tetanus, and to a second train (0.6 s at 180 Hz) to evoke the maximal tetanic force.

For measurement of fatigue, muscles were repeatedly stimulated in isotonic conditions with a series of 0.1 ms pulses (0.4 s at 120 Hz). When the isolated muscle was no longer able to shorten compared to the reference force (one-third of its maximum force) [32,33] the fatigue test was terminated.

A last isometric stimulus was performed to end the protocol and to determine whether the muscle was damaged after the fatigue sequence. Muscle specimens were weighed after removal of the tendons to calculate CSA values.

Statistics

Comparisons between multiple data sets were analyzed by ANOVA (One-way analysis of variance) with the Tukey multiple comparison post-tests. The Student t-test was used for comparisons between two data sets as immunodeficient mice versus immunocompetent mice. All data were analysed on GraphPad Prism 5.1 software (GraphPad Software, Inc., La Jolla, CA).

Results

Histological analysis of skeletal and cardiac muscles from *Sgcb/Rag2/γc*- null mice.

Fibrosis, fiber degeneration and calcification were present, mainly in muscles from ID-Sgcb null. Central nucleated fibers were seen in all dystrophic skeletal muscle sections (Fig. 1A, B). Muscle calcifications were observed directly in intact diaphragms from dystrophic mice compared to the wild-type and the Rag2/γc null mice (Fig. 1C). Fibrosis (Fig. 1D) and calcification (Fig. 1E) quantification were performed on H&E and in Masson's trichrome staining. In cardiac and diaphragm muscles of ID-Sgcb null mice, an increase of fibrosis was observed in respect to IC-Sgcb null mice, while comparable fibrosis was present in the hindlimb muscles of both ID-Sgcb null and IC-Sgcb null mice. The calcification areas were absent in control muscles whereas they were present in ID-Sgcb null mice compared to the IC-Sgcb null mice, in both skeletal and cardiac muscles.

The infiltration of macrophages M1 and M2, in the hindlimb muscle and heart, are reported in (Fig. 2A) as F4/80 positive and CD206 positive cells respectively. The cell quantification showed an increased amount of M1 in the hindlimb of ID-Sgcb null mice compared to controls and IC-Sgcb null mice (Fig. 2B). In the cardiac muscles, an increase of M2 macrophages in IC-Sgcb null compared to ID-Sgcb null mice and controls was observed (Fig. 2C). No differences were found in the M2/M1 ratio in both hindlimb and heart (Fig. 2D).

Type of fibres and functional comparison between IC-Sgcb null and ID-Sgcb null mice and with the controls

Immunostaining with specific antibodies was performed in cross-sections of gastrocnemius muscles from IC-Sgcb null, ID-Sgcb null and control mice. We were able to distinguish between slow oxidative fibres (Myh1 positive) and fast glycolytic type A (Myh2a positive Fig. 3). The fibre cross-sectional area (CSA) was measured and its percentage distribution, for both fast and slow fibres, is shown in Fig. 3. A statistically significant reduction of CSA was found in both dystrophic mice compared to controls in both fibre types, although more evident in ID-Sgcb null mice. NADH staining on the same samples showed comparable results and further allowed identification of slow oxidative fibres, fast oxidative type A and fast glycolitic type B (Supplementary Fig. 1). Quantification fibre cross-sectional area (CSA) and its percentage distribution showed again a significant reduction in IC and ID-Sgcb null mice compared to controls (Supplementary Fig. 1). Mean values of the main morphological parameters of EDL are reported with their standard deviation (sd) for both 1 and 7 months in Supplementary Table 1. However, no significant differences were observed.

Next, we measured the muscle strength of dystrophic and control mice with electrical stimulation. The mean of maximum forces measured during fused tetanus stimulation at 180Hz is reported in Fig. 4A. Maximum forces in 1-month-old samples were lower compared to 7-month-old samples. At 1 month, ID-Sgcb null EDL was impaired compared to wt and to IC-Sgcb null. No statistically differences were observed in 7-month-old dystrophic muscles and their maximum forces are significantly less compared to controls. T The specific force at 180Hz (Fig. 4B) showed a statistically significant decrease in ID-Sgcb null compared to IC-Sgcb null mice at 1 month of age but the difference disappears at 7 months of age. The specific force at 200Hz did not show statistically significant differences between the immunocompetent and immunodeficient dystrophic muscles (Fig. 4C)

The fatigue test, which shows the force decline only during 40 seconds of fatiguing stimulation, is reported in Fig. 4B. 1-month-old EDL muscles from ID-Sgcb null mice fatigued more rapidly compared to IC-Sgcb null and wt muscles. At 7months EDL muscles from both dystrophic mice fatigued with the same speed and more than wt muscles. Half relaxation tension, calculates with maximum and minimum forces, was statistically different between ID-Sgcb null and the IC-Sgcb null mice only at 1 month of age (Table 1).

MAB quantification and characterization in IC-Sgcb null, ID-Sgcb null and control mice.

The quantification of Mesoangioblasts (MABs) as AP-positive cells in both skeletal and cardiac muscle (Fig. 5B), showed a significant decrease in ID-Sgcb null mice compared to IC-Sgcb null mice at 7 months of age. We isolated a heterogeneous cell population by primary culture biopsies from both heart and hindlimb from 1 month and 7 months old mice. The amount of MABs, as AP+ cells, was calculated by enzymatic cytochemistry reaction staining that revealed purple positive cells (Fig. 5C, E). We detected no significant differences in the amount of positive purple cells from 1-month-old samples (Fig. 5D). However, a statistically significant increase of AP+ cells was observed in 7-month-old ID-Sgcb null samples compared to IC-Sgcb null samples (Fig. 5F). In general the number of MABs was reduced in 7-old-month biopsies of both heart and hindlimb compared to 1-month-old samples. FACS analysis of AP+ cells is reported Fig. 6. Due to the different sensitivity of the technique, the percentage of AP+ cells obtained by FACS is much less compared to the values obtained by the enzymatic staining. Nevertheless, AP+ cells in the heart of the C57/6J control mice are more than those sorted by the other animals (Supplementary Fig. 2A-C). Notably, the electrical stimulation of the muscle strength measuring instrument (300B actuator/transducer system, Aurora, Canada) impacted positively the number of MABs obtained from treated EDL muscles compared to contralateral untreated ones (Supplementary Fig. 3).

Finally, similar amounts of smooth muscle cells, as calponin and SMA positive cells were obtained from 1- and 7-month-old samples (Fig. 6A, B). However, smooth muscle differentiation potential among MAB interstitial subpopulations was more evident in dystrophic MABs compared to controls (Fig. 6C).

Discussion

Previous studies on immunodeficient DMD models showed that the loss of T and B cells improved muscle strength and reduced fibrosis in diaphragm and heart [34,35]. However, clear disadvantages of mdx-based dystrophic animal models are the normal life span of the animals and the revertant fibres that affect data interpretation. Indeed, in a study showed that *Rag2– Il2rb–Dmd–*mice, a non revertant mutant dystrophin mouse model lacking T, B, and NK cells, had higher CK levels compared to *mdx,* and *wt* strains [36]. In addition, a severe muscle phenotype was observed in Sgca-null/scid/beige mice [37], an animal model of LGMD type 2D where scid and beige mutations cause a lack of both T and B lymphocytes and a selective impairment of NK cell functions.

Despite controversy in the literature regarding the impact of the immune system in chronic dystrophic muscle degeneration, animal models to address this crucial issue in other form of dystrophies are missing. Thus, in this study C57/6J mouse models of LGMD2E have been considered in the presence or in the absence of functional immune system. To assess whether the differences found are consequences of the lack of the immune system and related to the dystrophic muscular degeneration, *wt* and immunodeficient mice have been employed for comparison studies.

In our study, we observed an increase in pathological features of dystrophies in ID-Sgcb null mice compared to IC-Sgcb null. Our results are consistent with other studies that have reported an increase in muscle fibrosis in ID dystrophic muscle [36,37]. Additionally, our data showed a significant increase in muscle calcification in ID-Sgcb skeletal and cardiac muscles, especially in the diaphragm where the areas of calcification are clearly evident in freshly isolated muscles. Ectopic muscle calcification has been described in muscular dystrophy, however, our work shows a significant increase of muscle calcification in dystrophic mice due to the absence of the immune system.

Interestingly, the number of macrophages in the hindlimb muscles are tripled in the ID-Sgcb null mice respect to the IC-Sgcb null mice and other controls, but they are highly decreased in the heart. Furthermore, in the skeletal muscle of both IC-Sgcb null and ID-Sgcb null animals the amount of M1 and M2 macrophages was comparable. These findings are consistent with a previously described accumulation of M1 and M2 macrophages in the skeletal muscle after injury, or in chronic degenerative model of skeletal muscle [38,39]. In the heart, however M2 macrophages are dramatically decreased in IC-Sgcb null mice compared to ID-Sgcb null ones. Notably, M2 macrophages are commonly associated with advanced stages of tissue repair and have an anti-inflammatory role further sustained by the factors secreted, such as TGFβ and IL-10 [40]. Moreover, a recent work has shown that M2 macrophages might play a substantial role in contribution to

regeneration of murine infarcted hearts [41]. In this light, a decrease of pro-regenerative macrophages in the heart of ID-Sgcb null mice might correlate with a worsening of the cardiomyopathy.

Despite all the histologically negative features, functional performance at 7 months of age, when the dystrophic disease is advanced, was not worse in ID-Sgcb null mice compared to IC-Sgcb null mice. Functional parameters, including absolute force and fatigue, showed the same loss of force in both dystrophic mouse models compared to controls. However, at 1 month of agemuscles from IC-Sgcb performed better than those from ID-Sgcb. We hypothesize that the differences observed in functional parameters of 1-month-old EDL muscles between the ID-Sgcb null and IC-Sgcb null are probably caused by an earlier onset of muscle impairment in the absence of immune system. It is likely that after several muscle degeneration/regeneration cycles occurred over 6 months this discrepancy is lost.

Different types of resident stem cells have been described as actively participating in tissue regeneration in the skeletal and cardiac muscle interstitia, including mesoangioblasts (MAB) [12,16]. MABs have been mainly studied for their myogenic abilities. Additionally, they differentiate very efficiently to smooth muscle cells in response to TGFβ [42]. Moreover it has been previously reported that MABs originating from the heart and the aorta of Sgcb null mice aberrantly differentiated into skeletal muscle cells both in vitro and in vivo when transplanted in infarcted heart [43]. Here we reported that the amount of MABs derived from 7 month old ID-Sgcb null mice was much lower compared to those from IC-Sgcb null mice. This is probably due to a faster depletion of the MAB cell pool in the immunodeficient dystrophic environment in an attempt to counteract muscle degeneration. Nevertheless, dystrophic MAB cultures from ID-Sgcb null and IC-Sgcb null mice show similar proliferation capability. This suggests that the proliferation of skeletal muscle MAB is not affected by long exposure to an immunodeficient environment. Finally, we also noted that the amount of MABs obtained from the biopsies subjected to electrical stimulation is statistically higher compared to unstimulated MABs, consistent with previous studies showing a positive effect on cell proliferation in muscle subjected to electrical stimulations [44].

We observed that the overall differentiation potential of skeletal muscle MABs to smooth muscle cells was much higher compared to cardiac MABs, indicating that the specific tissue turnover of the heart is much lower compared to skeletal muscle. Interestingly 90% of cardiac dystrophic MABs isolated from 1-month-old IC-Sgcb null mice fully differentiated into calponin/SMA double positive cells while only 20% did so from *wt* MABs. This strongly suggests that their differentiation potential is altered by the dystrophic environment that requires more vasculature progenitors for tissue repair. This likely accelerates their differentiation program and in the long run might be responsible for progenitor senescence [45].

In conclusion, we provide evidence that the immunodeficient system associated with the dystrophic phenotype results in an increase in areas of muscle calcification and a reduction in fibre size, without impairing EDL muscle performance. Another important aspect is the decrease in the number of M2 anti-inflammatory macrophages in immunodeficient dystrophic hearts. This could contribute to cardiac degeneration in Sgcb null mice. Thus, further analysis at a late stage of the disease is necessary to draw a complete picture of the immune system involvement in disease progression.

Abbreviations.
AP: alkaline phosphatase
CSA: cross section area
DGC: Dystrophin-glycoprotein complex
DMD: Duschene muscular dystrophy
EDL: extensor digitorum longus
FACS: Fluorescence-activated cell sorting
GCN: gastrocnemuis
H&E: heamatoxylin and eosin
IC-Sgcb null mice: immunocompetent Sgcb-null mice
ID- Sgcb null mice: immunodeficient Sgcb-null mice
LGMD2: Limb-girdle muscular dystrophies autosomal recessive
LGMD2E: Limb-girdle muscular dystrophies type 2E
MABs: Mesoangioblast
TcL: cytotoxic T lymphocytes
TGFβ: trasforming growth factof beta
ThL: helper T lymphocytes
TregL: regulatory T lymphocytes
αSMA: alpha-Smooth muscle actin

FIGURES

Figure 1. **Histological analysis of *gastrocnemius (GCN)*, *diaphragm (DIA)* and cardiac muscles from C57BL/6J, *Rag2/γc* null mice, IC-Sgcb null and ID-Sgcb null mice.** Paraffin sections were obtained from 7-month-old mice and stained with heamatoxylin and eosin (H&E) (**A**) and Masson's trichrome (**B**). Fibrosis, fiber degeneration and central nucleation of fibers are present only in dystrophic samples (***** and arrows respectively). Similarly, large areas of necrosis and mild fibrosis are seen in dystrophic cardiac muscles. Bar = 50 μm. Muscle calcifications (arrows) can be observed directly in intact diaphragms from dystrophic mice (**C**). Fibrosis quantification (mm^2) of gastrocnemius (GCN), diaphragm (DIA) and cardiac muscles is shown as mean ± sd in panel (**D**). Calcification in GCN muscles, DIA and cardiac muscles is reported as mean ± sd in (**E**). One-way ANOVA test: n=4, **p<0.05*; ***p<0.01*; ****p<0.001*.

Figure 2. **Inflammatory infiltration in skeletal muscle and cardiac muscles from C57BL/6, *Rag2/γc* null mice, IC-Sgcb null and ID-Sgcb null mice.** Muscle sections were obtained from 7-month-old mice. The distribution of macrophages type M1 and M2 is reported in (**A**). F4/80Ab was used to identify M1 macrophages (in red). CD206-Ab was used to detect M2 macrophages (in green). Nuclei were counterstained in blue with Hoechts, bar = 50 μm. M1 macrophage quantification (cells / mm^2) in hindlimb is shown as mean ± sd in (**B**); M2 macrophage quantification (cells / mm^2) in the heart is shown as mean ± sd in (**C**); ratio M2/M1 in hindlimb and heart in shown as mean ± sd in (**D).** One-way ANOVA test: n=4, ****p<0.001*.

Figure 3. **Immunofluorescence staining for fibre types from skeletal muscle sections of 7-months old C57BL/6, Rag2/γc null IC-Sgcb null and ID-Sgcb null mice.** Antibodies used for this immunostaining mark fibre type 1 (A) and fibre type 2A (B). Bar= 50μm. The fibre cross-sectional area (CSA) was measured and the distribution is shown as mean ± sd for both slow and glycolytic type A. Several sections from three mice for each cohort were evaluated. One-way ANOVA test: compared to IC-Sgcb ($) and compared to ID-Sgcb (*), n=3, **,$$ p<0.01;*** p<0.001; ****,$$$$ p<0.0001.

Figure 4. **Functional muscle analysis from C57BL/6J, *Rag2/γc* null mice, IC-Sgcb null and ID-Sgcb null mice.** The isometric force measured during a fused tetanus stimulation at 180Hz are reported in (**A**) as maximum force and their normalization by muscle cross-sectional is reported in (**B**) as specific force. Another specific force, calculated with stimulation at 200Hz, is reported in a bar chart in (**C**). The time course of force decline during 40 seconds of fatiguing stimulation is shown in (**D**) as fatigue. Data are shown as mean from 1month (panels on the left) and 7 months (panels on the right) old mice (n=5); (s) seconds, (ms) millisecond, (mN) milliNewton. One-way ANOVA test: C57BL/6J vs IC-Sgcb null (‡);**Rag2/γc** null vs ID-Sgcb null (§); IC-Sgcb null vs ID-Sgcb null (*). n=4, [‡‡, §§,**]*p<0.01*; [‡‡‡, §§§,***]*p<0.001*.

Figure 5. **Pericyte quantification from C57BL/6J, *Rag2/γc* null mice, IC-Sgcb null and ID-Sgcb null mice.** Anti-alkaline phosphatase Abs (red fluorophore) revealed pericytes in red in *GCN* sections. Nuclei are counterstained in blue with Hoechts (**A**). Bar = 25 μm. Quantification of alkaline phosphatase positive cells is reported in (**B**). Alkaline phosphatase enzymatic staining was performed on mix population obtained by primary culture of biopsies from hindlimb muscle and heart of 1 month (**C**) (bar = 25 μm) and 7 months (**E**) (bar = 10 μm) old mice. Quantification of the alkaline phosphatase positive cells in hindlimbs and hearts from 1 month (**D**) and 7 months (**F**) old mice is shown as mean ± SEM. One-way ANOVA test: n=5, **p<0.05*; ***p<0.01*; ****p<0.001*.

Figure 6. Smooth muscle differentiation of interstitial cells and pericytes from C57BL/6J, *Rag2/γc* null, IC-Sgcb null, and ID-Sgcb null mice. Quantification of alpha-SMA+, calponin+, alpha-SMA/calponin double positive and double negative cells from 1 (**A**) and 7 (**B**) months old mice is shown. Immunofluorescence analysis for alpha-SMA (red) and calponin (green) and quantification of positive cells derived from cardiac and hindlimb pericytes of 1 month old mice is reported in (**C**) One-way ANOVA test: n=5, *$p<0.05$; **$p<0.01$; ***$p<0.001$; t-test: *$p<0.05$; **$p<0.01$.

TABLE 1. Functional muscle analysis from C57BL/6J, *Rag2/γc* null mice, IC-Sgcb null and ID-Sgcb null mice. Maximum Force (F max), Relative Force (F rel), Specific Force (F spec) and half relaxation tension (1/2 relax tension) values ± s.d. are reported for 1 month and 7 month old mice. (mN) Millinewton. One-way ANOVA test: C57BL/6J vs IC-Sgcb null (‡); IC-Sgcb null vs ID-Sgcb null (*); n=4, ‡,*$p<0.05$; ‡‡,**$p<0.01$; ‡‡‡,***$p<0.001$.

Supplementary Table 1. EDL muscle characteristics in C57BL/6J, *Rag2/γc* null, IC-*Sgcb* null and ID-*Sgcb* null mice.

TABLE 1. Functional muscle analysis from C57BL/6J, *Rag2/γc* null mice, IC-*Sgcb* null and ID-*Sgcb* null mice.

Table 1				
1 month	**C57Bl/6J**	***Rag2/γc* null**	**IC-Sgcb null**	**ID-Sgcb null**
F max (mN)	6..16 ± 2.06	6.05 ± 0.11	6.35 ± 2.65	4.43 ± 1.52
F rel (mN)	2..05 ± 0.69	2.02 ± 0.04	2.12 ± 0.88	1.48 ± 0.51
F spec (mN)	1.72 ± 0.47	2.32 ± 1.03	2.79 ± 1.55	1.30 ± 0.69
1/2 relax tension (mN)	9.23 ± 5.85	2.69 ± 0.11	12.45 ± 4	1.84 ± 0.96 *
7 months	**C57Bl/6J**	***Rag2/γc* null**	**IC-Sgcb null**	**ID-Sgcb null**
F max (mN)	32.18 ± 2.03	29.72 ± 2.35	19.82 ± 4.86 ‡‡	22.97 ± 11.83
F rel (mN)	10.73 ± 0.68	9.91 ± 0.78	6.61 ± 1.62	7.66 ± 3.94
F spec (mN)	7.31 ± 1.93	6.43 ± 2.28	3.23 ± 1.37 ‡‡	4.22 ± 2.53
1/2 relax tension (mN)	15.79 ± 1.05	14.43 ± 1.13	9.45 ±2 .46 ‡‡	11.25 ± 5.83

1   Ozawa, E., Noguchi, S., Mizuno, Y., Hagiwara, Y. & Yoshida, M. From dystrophinopathy to sarcoglycanopathy: evolution of a concept of muscular dystrophy. *Muscle & nerve* **21**, 421-438 (1998).

2   Ervasti, J. M. & Campbell, K. P. A role for the dystrophin-glycoprotein complex as a transmembrane linker between laminin and actin. *The Journal of cell biology* **122**, 809-823 (1993).

3   Durbeej, M. *et al.* Disruption of the β-sarcoglycan gene reveals pathogenetic complexity of limb-girdle muscular dystrophy type 2E. *Molecular cell* **5**, 141-151 (2000).

4   Wheeler, M. T. & McNally, E. M. Sarcoglycans in vascular smooth and striated muscle. *Trends in cardiovascular medicine* **13**, 238-243 (2003).

5   Coral-Vazquez, R. *et al.* Disruption of the sarcoglycan–sarcospan complex in vascular smooth muscle: a novel mechanism for cardiomyopathy and muscular dystrophy. *Cell* **98**, 465-474 (1999).

6   Hermans, M. *et al.* Hereditary muscular dystrophies and the heart. *Neuromuscular Disorders* **20**, 479-492 (2010).

7   Bönnemann, C. G. *et al.* β–sarcoglycan (A3b) mutations cause autosomal recessive muscular dystrophy with loss of the sarcoglycan complex. *Nature genetics* **11**, 266-273 (1995).

8   McNally, E. M. *et al.* Mutations that disrupt the carboxyl-terminus of γ-sarcoglycan cause muscular dystrophy. *Human molecular genetics* **5**, 1841-1847 (1996).

9   Durbeej, M. & Campbell, K. P. Muscular dystrophies involving the dystrophin–glycoprotein complex: an overview of current mouse models. *Current opinion in genetics & development* **12**, 349-361 (2002).

10   Cossu, G. & Biressi, S. in *Seminars in cell & developmental biology.* 623-631 (Elsevier).

11   Montarras, D. *et al.* Direct isolation of satellite cells for skeletal muscle regeneration. *Science* **309**, 2064-2067 (2005).

12   Dellavalle, A. *et al.* Pericytes of human skeletal muscle are myogenic precursors distinct from satellite cells. *Nature cell biology* **9**, 255-267 (2007).

13   Sampaolesi, M. *et al.* Mesoangioblast stem cells ameliorate muscle function in dystrophic dogs. *Nature* **444**, 574 (2006).

14   Minasi, M. G. *et al.* The meso-angioblast: a multipotent, self-renewing cell that originates from the dorsal aorta and differentiates into most mesodermal tissues. *Development* **129**, 2773-2783 (2002).

15   Sampaolesi, M. *et al.* Cell therapy of α-sarcoglycan null dystrophic mice through intra-arterial delivery of mesoangioblasts. *Science* **301**, 487-492 (2003).

16   Galvez, B. *et al.* Cardiac mesoangioblasts are committed, self-renewable progenitors, associated with small vessels of juvenile mouse ventricle. *Cell Death & Differentiation* **15**, 1417-1428 (2008).

17   Joe, A. W. *et al.* Muscle injury activates resident fibro/adipogenic progenitors that facilitate myogenesis. *Nature cell biology* **12**, 153 (2010).

18   Wynn, T. A. Fibrotic disease and the TH1/TH2 paradigm. *Nature Reviews Immunology* **4**, 583-594 (2004).

19   Li, L., Sad, S., Kägi, D. & Mosmann, T. R. CD8Tc1 and Tc2 cells secrete distinct cytokine patterns in vitro and in vivo but induce similar inflammatory reactions. *The Journal of Immunology* **158**, 4152-4161 (1997).

20   Spencer, M. J., Montecino-Rodriguez, E., Dorshkind, K. & Tidball, J. G. Helper (CD4+) and cytotoxic (CD8+) T cells promote the pathology of dystrophin-deficient muscle. *Clinical immunology* **98**, 235-243 (2001).

21   Morrison, J., Lu, Q. L., Pastoret, C., Partridge, T. & Bou-Gharios, G. T-cell-dependent fibrosis in the mdx dystrophic mouse. *Laboratory investigation* **80**, 881 (2000).

22   Burzyn, D. *et al.* A special population of regulatory T cells potentiates muscle repair. *Cell* 155, 1282-1295 (2013).

23   Ren, G., Michael, L. H., Entman, M. L. & Frangogiannis, N. G. Morphological characteristics of the microvasculature in healing myocardial infarcts. *Journal of Histochemistry & Cytochemistry* 50, 71-79 (2002).

24   Dobaczewski, M. *et al.* Vascular mural cells in healing canine myocardial infarcts. *Journal of Histochemistry & Cytochemistry* 52, 1019-1029 (2004).

25   Zymek, P. *et al.* The role of platelet-derived growth factor signaling in healing myocardial infarcts. *Journal of the American College of Cardiology* 48, 2315-2323 (2006).

26   Berardi, E. *et al.* Skeletal muscle is enriched in hematopoietic stem cells and not inflammatory cells in cachectic mice. *Neurological research* 30, 160-169 (2008).

27   Quattrocelli, M. *et al.* Mesodermal iPSC–derived progenitor cells functionally regenerate cardiac and skeletal muscle. *The Journal of clinical investigation* 125, 4463-4482 (2015).

28   Vandenboom, R., Hannon, J. D. & Sieck, G. C. Isotonic force modulates force redevelopment rate of intact frog muscle fibres: evidence for cross-bridge induced thin filament activation. *The Journal of physiology* 543, 555-566 (2002).

29   Martonosi, A. N. Animal electricity, Ca2+ and muscle contraction. A brief history of muscle research. *Acta Biochimica Polonica* 47, 493-516 (2000).

30   Brooks, S. V. & Faulkner, J. A. Contractile properties of skeletal muscles from young, adult and aged mice. *The Journal of physiology* 404, 71-82 (1988).

31   Hill, A. The effect of load on the heat of shortening of muscle. *Proceedings of the Royal Society of London B: Biological Sciences* 159, 297-318 (1964).

32   Emslie-Smith, A. M., Arahata, K. & Engel, A. G. Major histocompatibility complex class I antigen expression, immunolocalization of interferon subtypes, and T cell-mediated cytotoxicity in myopathies. *Human pathology* 20, 224-231 (1989).

33   Seow, C. & Stephens, N. Fatigue of mouse diaphragm muscle in isometric and isotonic contractions. *Journal of Applied Physiology* 64, 2388-2393 (1988).

34   Farini, A. *et al.* Novel insight into stem cell trafficking in dystrophic muscles. *International journal of nanomedicine* 7, 3059 (2012).

35   Farini, A. *et al.* T and B lymphocyte depletion has a marked effect on the fibrosis of dystrophic skeletal muscles in the scid/mdx mouse. *The Journal of pathology* 213, 229-238 (2007).

36   Vallese, D. *et al.* The Rag2–Il2rb–Dmd–mouse: a novel dystrophic and immunodeficient model to assess innovating therapeutic strategies for muscular dystrophies. *Molecular Therapy* 21, 1950-1957 (2013).

37   Gerli, M. F., Maffioletti, S. M., Millet, Q. & Tedesco, F. S. Transplantation of induced pluripotent stem cell-derived mesoangioblast-like myogenic progenitors in mouse models of muscle regeneration. *Journal of visualized experiments: JoVE* (2014).

38   Novak, M. L., Weinheimer-Haus, E. M. & Koh, T. J. Macrophage activation and skeletal muscle healing following traumatic injury. *The Journal of pathology* 232, 344-355 (2014).

39   Kharraz, Y., Guerra, J., Mann, C. J., Serrano, A. L. & Muñoz-Cánoves, P. Macrophage plasticity and the role of inflammation in skeletal muscle repair. *Mediators of inflammation* 2013 (2013).

40   Bosurgi, L. *et al.* Transplanted mesoangioblasts require macrophage IL-10 for survival in a mouse model of muscle injury. *The Journal of Immunology* 188, 6267-6277 (2012).

41   Shiraishi, M. *et al.* Alternatively activated macrophages determine repair of the infarcted adult murine heart. *The Journal of clinical investigation* 126, 2151-2166 (2016).

42   Tagliafico, E. *et al.* TGFβ/BMP activate the smooth muscle/bone differentiation programs in mesoangioblasts. *Journal of cell science* 117, 4377-4388 (2004).

43   Crippa, S. *et al.* miR669a and miR669q prevent skeletal muscle differentiation in postnatal cardiac progenitors. *The Journal of cell biology* 193, 1197-1212 (2011).

44   Maziarz, A. *et al.* How electromagnetic fields can influence adult stem cells: positive and negative impacts. *Stem cell research & therapy* 7, 54 (2016).

45   Blau, H. M., Cosgrove, B. D. & Ho, A. T. The central role of muscle stem cells in regenerative failure with aging. *Nature medicine* 21, 854 (2015).
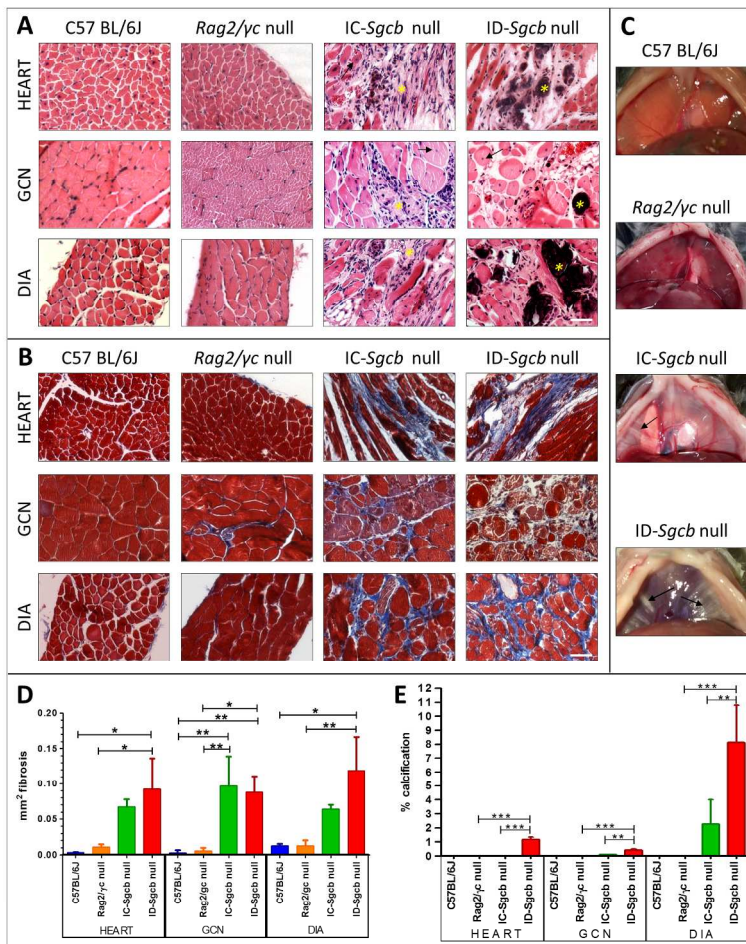
Figure 1

Figure 1

180x259mm (300 x 300 DPI)
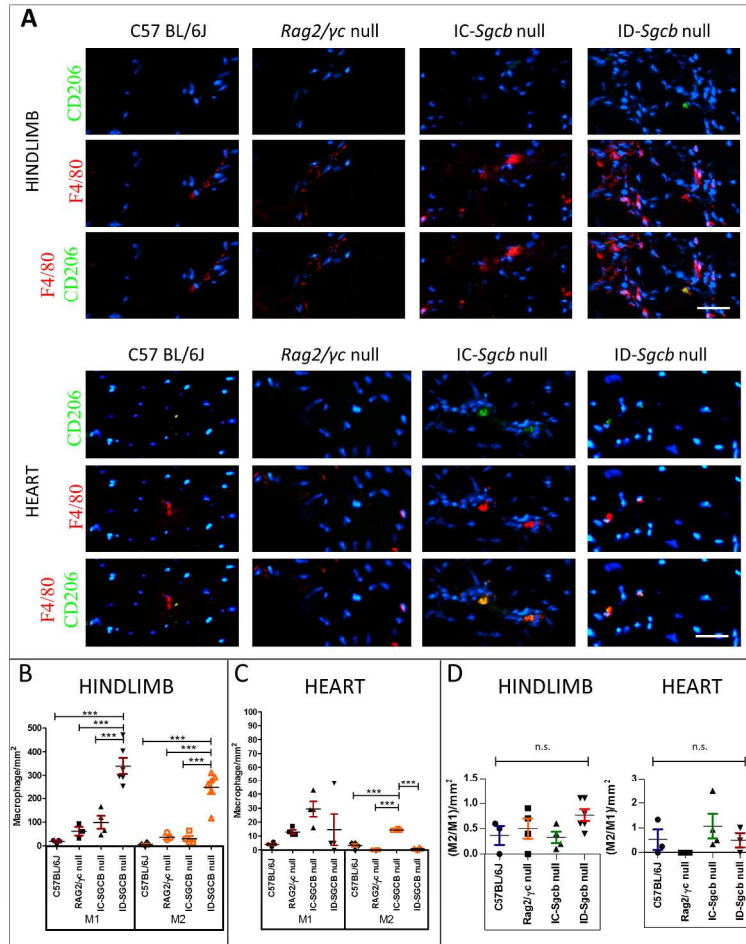
Figure 2

Figure 2

180x259mm (300 x 300 DPI)
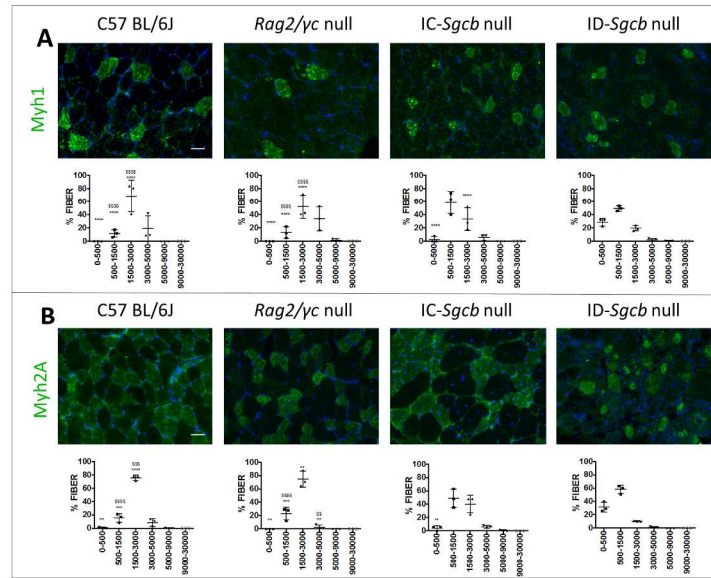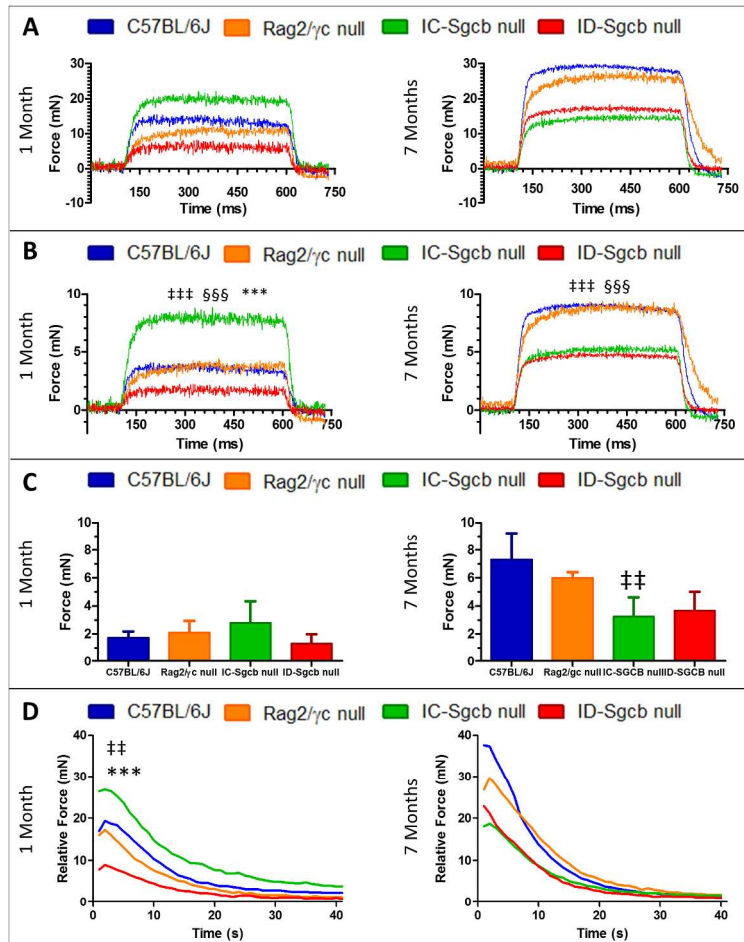
Figure 4

Figure 4

180x259mm (300 x 300 DPI)
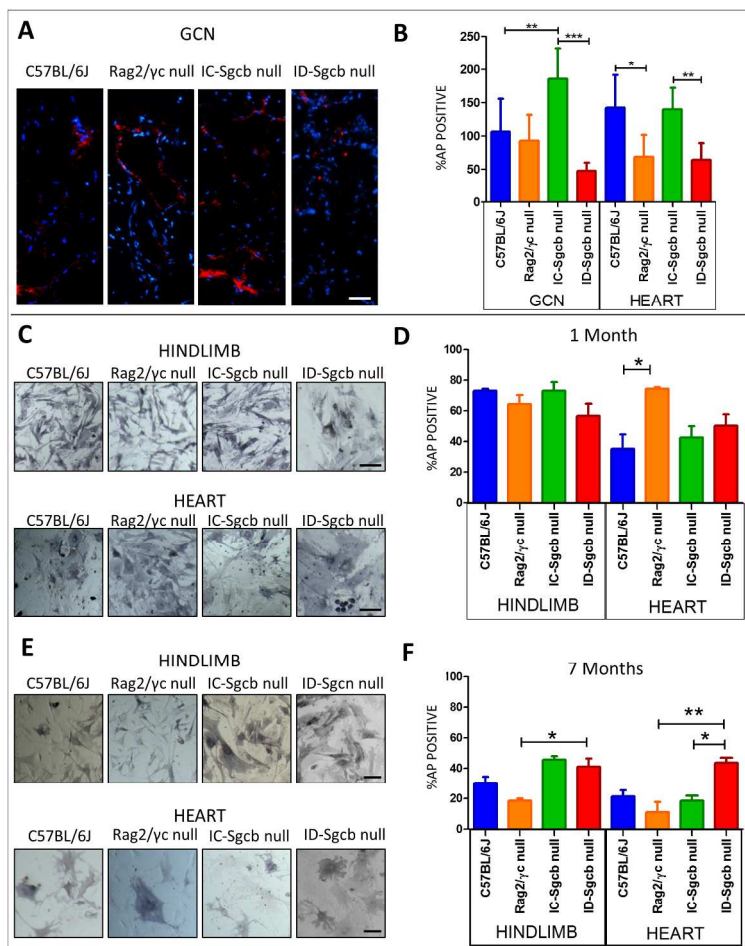
Figure 5

Figure 5

180x259mm (300 x 300 DPI)
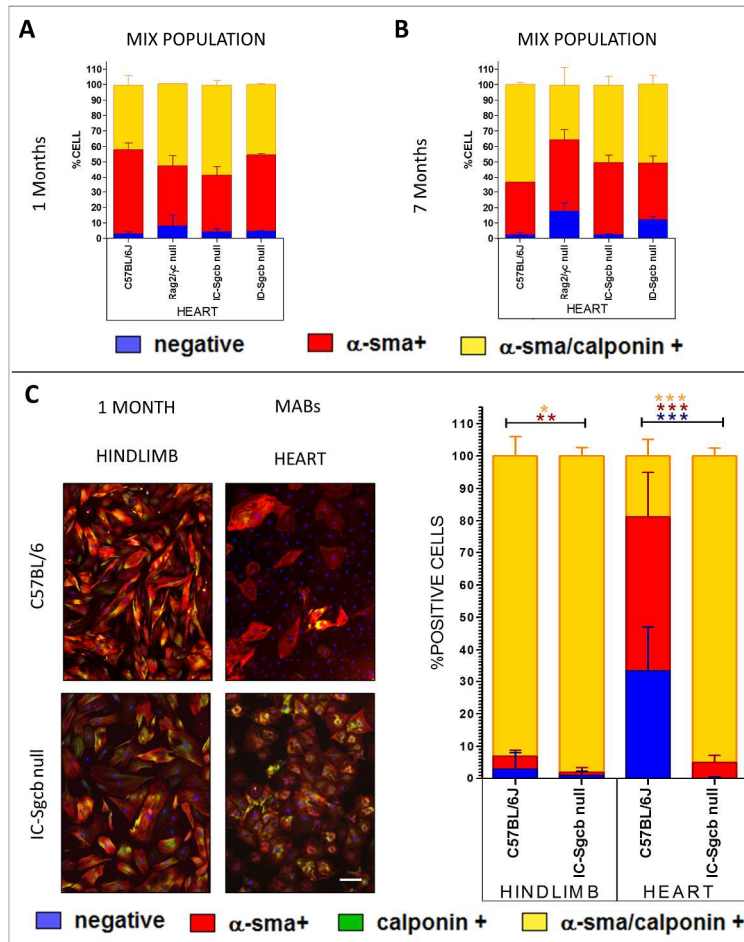
Figure 6

Figure 6

180x259mm (300 x 300 DPI)